

Search for a vortex loop blowout transition in a type-II superconductor in a finite magnetic field

P. Olsson

Department of Theoretical Physics, Umeå University, 901 87 Umeå, Sweden

S. Teitel

Department of Physics and Astronomy, University of Rochester, Rochester, NY 14627

(Received 26 November 2002; published 25 April 2003)

The three-dimensional uniformly frustrated XY model is simulated to search for a predicted “vortex loop” transition within the vortex line liquid phase of a strongly type-II superconductor in an applied magnetic field. Results are shown to strongly depend on the precise scheme used to trace out vortex line paths. While we find evidence for a transverse vortex path percolation transition, no signal of this transition is found in the specific heat.

DOI: 10.1103/PhysRevB.67.144514

PACS number(s): 74.72.-h, 74.25.Dw

I. INTRODUCTION

In pure extreme type-II superconductors, such as the high- T_c superconductors, the Abrikosov vortex line lattice melts via a sharp first-order phase transition¹ into a vortex line liquid as the temperature is increased above a critical T_m . The properties of this vortex line liquid phase have been the subject of considerable investigation. Theoretical arguments² and early simulations^{3–5} suggested that the vortex line liquid might retain superconducting phase coherence parallel to the applied magnetic field, within some temperature interval above T_m . Later, better converged simulations⁶ found that phase coherence is simultaneously lost in all directions upon melting.

Subsequently, Tešanović⁷ proposed that, for small magnetic fields, there still remains a sharp thermodynamic phase transition at a temperature T_Φ within the vortex liquid state, associated with diverging fluctuations of closed vortex loops, such as drive the superconducting transition in the zero magnetic-field case. Considering the limit of infinite penetration length λ , Tešanović proposed that, in a finite field, the fluctuations of the magnetic-field-induced vortex lines act to screen the interactions of thermally excited closed vortex loops, in the same way that magnetic-field fluctuations screen the vortex loop interactions of a finite λ model in zero applied magnetic field. Pursuing this argument, he predicted that the proposed vortex loop “blowout” transition at T_Φ may be an inverted XY transition, as is the case of the zero-field Meissner transition for the finite λ model. Suggestions of such a vortex loop blowout transition had earlier been claimed in simulations by Ryu and Stroud.⁵

Following Tešanović’s predictions, Nguyen and co-workers^{8–10} carried out numerical simulations of the three-dimensional (3D) uniformly frustrated XY model of a type-II superconductor. They claimed to find evidence for Tešanović’s transition, which they associated with the formation of a vortex line path that percolates entirely around the system in the direction transverse to the magnetic field.

Most recently, measurements¹¹ on high-purity $\text{YBa}_2\text{Cu}_3\text{O}_7$ (YBCO) single crystals produced evidence of a steplike anomaly in the specific heat at a temperature higher than the melting T_m , reminiscent of an inverted mean-field transition. It has been argued¹¹ that this feature may be evi-

dence for Tešanović’s transition T_Φ .

In order to further investigate this issue, we have carried out new simulations on the 3D uniformly frustrated XY model, both repeating the approach of Nguyen and co-workers, and measuring new quantities that make a more direct test of Tešanović’s theory. After correcting certain inconsistencies in the earlier numerical work, we show that whether or not one finds indications of a vortex loop blowout transition depends crucially on how one chooses to resolve vortex line paths at points where two or more lines intersect. Making the choice that favors the blowout interpretation, we find the critical exponent $\nu \approx 1$, rather than the value $\sim 2/3$ expected for an inverted 3D XY transition. Finally, we make high-precision measurements of the specific heat, in search of a thermodynamic signature for a blowout transition, but no such signature is found.

II. MODEL

The model that we use is the 3D uniformly frustrated XY model,^{3–6,8–10,12} which models a type-II superconductor in the limit of infinite magnetic penetration length, $\lambda \rightarrow \infty$, and is given by the Hamiltonian

$$\mathcal{H}[\theta_i] = - \sum_{i,\mu} J_\mu \cos(\theta_{i+\hat{\mu}} - \theta_i - A_{i\mu}). \quad (1)$$

Here i are the nodes of a cubic grid of sites, $\mu = x, y, \text{ and } z$ are the directions of the grid axes; and the sum is over all nearest-neighbor bonds of the grid. θ_i is the phase angle of the superconducting wave function on site i , $A_{i\mu} = (2\pi/\Phi_0) \int_i^{i+\hat{\mu}} \mathbf{A} \cdot d\mathbf{r}$ is given by the integral of the magnetic vector potential \mathbf{A} across the bond at site i in direction $\hat{\mu}$, and $\Phi_0 = hc/2e$ is the flux quantum. The argument of the cosine is the gauge-invariant phase angle difference across the bond. The circulation of the $A_{i\mu}$ around any plaquette of the grid is equal to 2π times the number of flux quanta of magnetic field penetrating the plaquette. We take the magnetic field, $\mathbf{B} = \nabla \times \mathbf{A}$, uniform and parallel to the \hat{z} axis, with a fixed density of flux quanta $f = Ba^2/\Phi_0$ per plaquette of area a^2 . We take the couplings J_μ to model an anisotropic system, with $J_x = J_y \equiv J_\perp$ and $J_z \leq J_\perp$.

Simulations were carried out varying the θ_i according to a usual Monte Carlo scheme; the $A_{i\mu}$ were held fixed. That the $A_{i\mu}$ do not fluctuate, and that they give a uniform magnetic field, are the consequences of the $\lambda \rightarrow \infty$ approximation. Simulations were carried out on $L_z \times L_\perp^2$ cubic grids, using periodic boundary conditions. Except where otherwise noted, our runs were typically for $1/4$ to $1/2 \times 10^6$ Monte Carlo passes through the entire lattice.

While we simulate in the phase angle degrees of freedom, θ_i , our interest lies in the behavior of the vorticity in these phase angles. Let s denote the *dual* sites of the original grid; these are the sites at the centers of the unit cells of the grid. We denote by (s, μ) the plaquette which is the face of the unit cell centered on dual site s , with normal in the $\hat{\mu}$ direction, $\mu = x, y$, and z . We define the integer vorticity $n_{s\mu}$ piercing plaquette (s, μ) by computing the circulation of the gauge-invariant phase angle differences around the plaquette,

$$\sum_{(s, \mu)} [\theta_{i+\hat{\sigma}} - \theta_i - A_{i\sigma}] = 2\pi(n_{s\mu} - f\delta_{z\mu}), \quad (2)$$

where the sum is counterclockwise around all bonds forming the boundary of plaquette (s, μ) , and the gauge-invariant phase angle differences are restricted to the interval $(-\pi, \pi)$. In a constant magnetic field, the condition that the total-energy density remains finite can be shown to yield the ‘‘neutrality’’ constraint (see Sec. III A),

$$\sum_s n_{s\mu} = fL_\perp^2 L_z \delta_{z\mu}, \quad (3)$$

i.e., the total vorticity piercing any plane at constant z is fL_\perp^2 ; these are the magnetic-field-induced vortex lines. The total vorticity in the transverse directions x and y is zero.

Taking the vorticity $n_{s\mu}$ as the directed bond of the dual grid, emanating from site s in direction $\hat{\mu}$, the vorticity so defined is divergenceless, forming continuous lines that, due to the periodic boundary conditions, must ultimately close upon themselves. We will label such a closed vortex path by the index α , and define the vector \mathbf{R}_α as the net displacement one travels upon following the path α from a given starting point until returning back to that point as the line closes back on itself. If $\mathbf{R}_\alpha = 0$, then the vortex line path is a closed loop of finite extent that exists as a thermal fluctuation. If $R_{z\alpha} = mL_z$, with m an integer, then such a vortex line path represents m of the fL_\perp^2 field-induced vortex lines; these m lines are mutually connected to each other via the periodic boundary conditions in the z direction.⁴ For $m > 1$, we can say that the m field-induced lines are geometrically entangled with each other. If $R_{x\alpha} = mL_\perp$ or $R_{y\alpha} = mL_\perp$, then the vortex line path winds m times around the system *transversely* to the applied magnetic field. We will be particularly interested in vortex line paths for which $R_{z\alpha} = 0$, but $R_{x\alpha}$ or $R_{y\alpha} \neq 0$. The set of vortex line paths $\{\alpha\}$ for which all $R_{z\alpha} > 0$; we will henceforth refer to as the ‘‘lines;’’ these are the field-induced vortex lines. All other vortex paths we will refer to as the ‘‘loops.’’

In order to trace vortex line paths, one needs to know the way to treat intersections. An intersection occurs when there

is more than one vortex line entering and exiting a give unit cell of the grid; it is therefore ambiguous which entering segment to connect to which exiting segment. It was previously shown¹³ by one of us that the method chosen to resolve such intersections can have a dramatic effect on the statistics of closed thermally excited loops in the zero-field $f=0$ model. Here, for the $f > 0$ model, we consider two different schemes, which we henceforth refer to as method (i) and method (ii):

(i) At each intersection we choose randomly, with equal probability, which entering segment connects to which exiting segment. In the $f=0$ model this scheme was found to give results closest to theoretical expectations.¹³

(ii) Motivated by Nguyen and co-workers,^{8–10} we first search¹⁴ through all possible connections to find a path α with $R_{z\alpha} = 0$ and $R_{x\alpha}$ or $R_{y\alpha} \neq 0$. Such a path winds around the system transverse to the field, without ever winding around the system parallel to the field. If one such path is found, it is selected as a path α' contributing to the ‘‘loops,’’ and we then repeat the procedure applied to all remaining vortex paths. When all such transverse paths are found, the remaining vortex line intersections are resolved randomly, as in method (i).

Using either method (i) or method (ii) we thus decompose the vorticity of any given configuration into disjoint closed vortex line paths, consisting of a set $\{\alpha\}$ of ‘‘lines’’ and a set $\{\alpha'\}$ of ‘‘loops.’’

III. WINDING OF FIELD-INDUCED VORTEX LINES

We first attempt a direct test of Teřanović’s theory of the T_Φ transition within the liquid phase. A summary of his arguments for the existence of this transition is as follows.

A. Summary of Teřanović’s theory

First, a duality transformation^{15–17} from the XY model of Eq. (1) gives the interaction between vortices as

$$\mathcal{H}[n_{s\mu}] = \frac{1}{2} \sum_{s, s', \mu} [n_{s\mu} - f\delta_{z\mu}] V^\mu(\mathbf{r}_s - \mathbf{r}_{s'}) [n_{s'\mu} - f\delta_{z\mu}], \quad (4)$$

where $V^\mu(\mathbf{r})$ is the appropriate anisotropic generalization of the Coulomb interaction, with Fourier transform $V_q^\mu \sim q^{-2}$. It is this singularity of V_q^μ as $q \rightarrow 0$ that yields the constraint of Eq. (3).

Next, one imagines decomposing the total vorticity of the system into lines and loops,

$$n_{s\mu} = n_{s\mu}^{\text{lines}} + n_{s\mu}^{\text{loops}}. \quad (5)$$

If we define

$$b_{s\mu} \equiv n_{s\mu}^{\text{lines}} - f\delta_{z\mu}, \quad (6)$$

then $\sum_s \langle b_{s\mu} \rangle = 0$ and the Hamiltonian of Eq. (4) can be rewritten as

$$\mathcal{H} = \frac{1}{2} \sum_{s, s', \mu} [n_{s\mu}^{\text{loops}} - b_{s\mu}] V^\mu(\mathbf{r}_s - \mathbf{r}_{s'}) [n_{s'\mu}^{\text{loops}} - b_{s'\mu}]. \quad (7)$$

Tešanović then argued that a coarse graining of vortex fluctuations, in the vortex line liquid phase, leads to an effective hydrodynamic Hamiltonian on long length scales which has the same interaction piece as Eq. (7), but which has a new additive term proportional to $\sum_{s\mu} b_{s\mu}^2$. The resulting long length scale Hamiltonian then has exactly the same form as that of a zero-field superconductor with thermally fluctuating vortex loops, $n_{s\mu}^{\text{loops}}$, and a thermally fluctuating magnetic field $b_{s\mu}$ whose average is zero, i.e., the zero-field superconductor with a finite penetration length λ . In other words, in this *infinite* λ theory at *finite* magnetic field, the long-wavelength fluctuations of the field-induced vortex lines $n_{s\mu}^{\text{lines}}$ screen the interaction between the vortex loops $n_{s\mu}^{\text{loops}}$ in exactly the same manner as magnetic-field fluctuations screen the interactions between vortex loops in a *finite* λ model at *zero* magnetic field.

The Meissner transition at T_c in the zero-field, finite λ , model is an *inverted* 3D XY transition.¹⁵ The high-temperature phase $T > T_c$ has vortex loops on all length scales and breaks a global U(1) symmetry associated with a *disorder* parameter;¹⁸ the low-temperature phase $T < T_c$ has no vortex loops on sufficiently long length scales. The correlation length ξ and renormalized magnetic penetration length λ_R both diverge¹⁹ as $\sim |t|^{-\nu}$, with $\nu \approx 2/3$ and $t \equiv T - T_c$.

Earlier we have carried out numerical simulations¹⁹ of this zero-field, finite λ , Meissner transition. We demonstrated that, in this model, magnetic-field fluctuations obey the finite-size scaling relation

$$F(t, q, L) \equiv \langle b_\mu(q\hat{\nu}) b_\mu(-q\hat{\nu}) \rangle / L^3 \sim L^{-1} F(tL^{1/\nu}, qL, 1), \quad (8)$$

where in the above $\hat{\mu} \perp \hat{\nu}$ and $b_\mu(q\hat{\nu}) = \sum_s e^{-iq\hat{\nu} \cdot \mathbf{r}_s} b_{s\mu}$ is the Fourier transform of the magnetic-flux density $b_{s\mu}$. As $L \rightarrow \infty$, and $q \rightarrow 0$,

$$F(t, 0, \infty) \sim \begin{cases} 0 & t < 0, \\ 1/\xi & t > 0, \end{cases} \quad (9)$$

hence $F(t, 0, \infty)$ vanishes below the transition, and increases continuously from zero as one goes above the transition.

In the present case of a finite magnetic field, if Tešanović's mapping is correct, the Meissner transition T_c becomes the transition T_Φ within the vortex line liquid phase, and we expect the exact same scaling as that in Eq. (8) above, when applied to the quantity $b_{s\mu}$ defined in Eq. (6). Taking the limit of $q \rightarrow 0$ in Eq. (8), and applying to systems with fixed aspect ratio $L_z = gL_\perp$, we expect the scaling

$$\left\langle \left(\sum_s b_{s\mu} \right)^2 \right\rangle / L_\perp^3 \sim L_\perp^{-1} f(tL_\perp^{1/\nu}), \quad (10)$$

where $t \equiv T - T_\Phi$ and $f(x) = F(x, 0, 1)$.

For the directions $\hat{\mu} = \hat{x}$ or \hat{y} ,

$$\sum_s b_{s\mu} = \sum_s n_{s\mu}^{\text{lines}} \equiv W_\mu L_\perp \quad (11)$$

is the net vorticity of the magnetic-field-induced vortex lines in the transverse direction $\hat{\mu}$. The two-dimensional vector $\mathbf{W} = (W_x, W_y)$ defined above is the integer-valued ‘‘winding number’’ that counts the net number of times the field-induced vortex lines wind around the system in the transverse directions \hat{x} and \hat{y} . If $\{\alpha\}$ is the set of vortex line paths that define the field-induced vortex lines $n_{s\mu}^{\text{lines}}$, and \mathbf{R}_α is the net displacement along path α as defined earlier, then $\sum_\alpha \mathbf{R}_{\alpha\perp} = \mathbf{W} L_\perp$, where $\mathbf{R}_\perp \equiv (R_x, R_y)$. We thus expect from Eq. (10) the finite-size scaling

$$\langle W^2 \rangle \sim f(tL_\perp^{1/\nu}). \quad (12)$$

Note that the neutrality condition of Eq. (3) implies that the *total* transverse vorticity in the system must always vanish. For $\mathbf{W} \neq 0$, it is therefore necessary that any such winding of the field-induced lines is exactly canceled out by an equal and opposite transverse winding of the loops. In the thermodynamic limit, $L_\perp \rightarrow \infty$, Eq. (9) implies that $\langle W^2 \rangle = 0$ for $T < T_\Phi$, and $\langle W^2 \rangle$ increases continuously from zero as one increases $T > T_\Phi$. The proposed transition at T_Φ is thus associated with the appearance of infinite transverse loops (see following Sec. IV).

Another interpretation of the T_Φ transition follows from the ‘‘two-dimensional (2D) boson’’ model²⁰ of interacting vortex lines, in which the field-induced vortex lines are viewed as the world lines of two-dimensional bosons traveling down the imaginary time axis. For $T < T_\Phi$ where $\langle W^2 \rangle = 0$, the field-induced vortex lines behave like *charged* two-dimensional bosons,^{2,17} with a long-range retarded Coulomb interaction. In the vortex line liquid, $T_m < T < T_\Phi$, where phase coherence is lost parallel to the applied magnetic field, the analog 2D bosons are in a *charged* superfluid state. For $T > T_\Phi$, where $\langle W^2 \rangle \neq 0$, screening by the infinitely large loops $n_{s\mu}^{\text{loops}}$ results in an effective short-range interaction between the field-induced lines. In this case the winding number squared $\langle W^2 \rangle$ is proportional to the superfluid density of what is now an *uncharged* superfluid. Thus T_Φ corresponds to a transition between a charged superfluid and an uncharged superfluid in the analog 2D boson theory. Equivalently, if one considers the quanta that mediate the interaction between the analog 2D bosons, the transition is from massless quanta for $T < T_\Phi$ to massive quanta for $T > T_\Phi$.

To arrive at Eq. (12), we considered the transverse components of Eq. (10). However, we can also consider the parallel, $\hat{\mu} = \hat{z}$ component. Now,

$$\sum_s b_{sz} = \sum_s n_{sz}^{\text{lines}} - fL_\perp^2 L_z \equiv W_z L_z, \quad (13)$$

and so we expect the scaling

$$\langle W_z^2 \rangle \sim f_z(tL_\perp^{1/\nu}). \quad (14)$$

If $\{\alpha\}$ is the set of vortex line paths that define the field-induced vortex lines $n_{s\mu}^{\text{lines}}$, and \mathbf{R}_α is the net displacement along path α as defined earlier, then $\sum_\alpha R_{\alpha z} = (fL_\perp^2 + W_z) L_z$. Thus W_z gives the number of ‘‘lines’’ in excess of the average value fL_\perp^2 set by the applied magnetic field. The

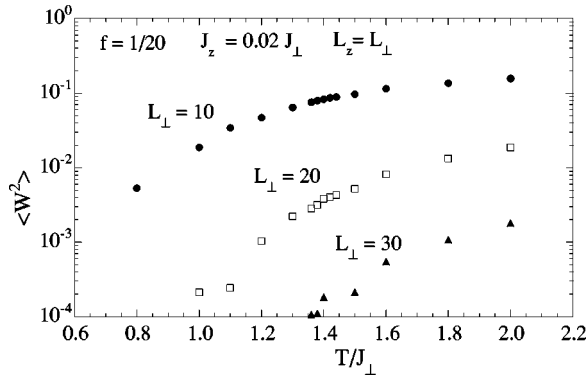


FIG. 1. Semilog plot of winding $\langle W^2 \rangle$ vs T/J_{\perp} for $L_{\perp} = 10, 20,$ and 30 , with vortex density $f = 1/20$, anisotropy $J_z = 0.02J_{\perp}$, and aspect ratio $L_z = L_{\perp}$. $\langle W^2 \rangle$ is computed using method (i), i.e., random connections at intersections. $\langle W^2 \rangle$ steadily decreases as L_{\perp} increases, over the entire temperature range.

neutrality condition of Eq. (3) requires that when $W_z > 0$, there must be an equal and opposite parallel winding of the loops $n_{s\mu}^{\text{loops}}$. As $L \rightarrow \infty$, we have $W_z = 0$ for $T < T_{\Phi}$, and $W_z > 0$ for $T > T_{\Phi}$. Thus a transition at T_{Φ} should be characterized by fluctuations in the number of field-induced lines and by the appearance of infinite parallel loops directed opposite to the direction of the applied magnetic field.

B. Numerical results

To test the above predictions, we have simulated the 3D uniformly frustrated XY model of Eq. (1) using a vortex density $f = 1/20$, anisotropy $J_z/J_{\perp} = 0.02$, and aspect ratio $L_z/L_{\perp} = 1$, for $L_{\perp} = 10, 20, 30, 40,$ and 60 . For these parameters, the vortex lattice melting temperature is $T_m \approx 0.24J_{\perp}$, and the zero-field critical temperature is $T_{c0} \approx 1.14J_{\perp}$. We compute the transverse winding \mathbf{W} of the field-induced lines, defined by Eq. (11), using both method (i) and method (ii) to decompose each configuration into “lines” and “loops.” According to the scaling Eq. (12), we expect that plots of $\langle W^2 \rangle$ vs T for different sizes L_{\perp} should all intersect at the common point $t = 0$, or $T = T_{\Phi}$.

In Fig. 1 we show a semilog plot of $\langle W^2 \rangle$ vs T/J_{\perp} using method (i) (random reconnections at intersections) for $L_{\perp} = 10, 20,$ and 30 . We see that there is clearly no common intersection point of the curves. As L_{\perp} increases, $\langle W^2 \rangle$ decreases uniformly over the entire temperature range. This is in qualitative agreement with earlier computations of $\langle W^2 \rangle$ by one of us (see Fig. 15 of Ref. 4). For $L_{\perp} = 60$, we have found no net transverse winding of the field-induced lines at all, i.e., for the length of our simulation we had $\mathbf{W} = 0$, for the temperature range $1.36 \leq T/J_{\perp} \leq 1.44$.

Next, in Fig. 2, we show the same quantities but now using method (ii) (search first for maximal transverse loops), for $L_{\perp} = 10, 20, 30, 40,$ and 60 . We see that as L_{\perp} increases, the curves seem to approach a common intersection point, giving $T_{\Phi} \approx 1.4J_{\perp}$. Note that this T_{Φ} is above the zero-field critical temperature $T_{c0} \approx 1.14J_{\perp}$.

From Eq. (12), we expect that the slopes of these curves at T_{Φ} should scale with system size as $d\langle W^2 \rangle/dT \sim L_{\perp}^{1/\nu}$.

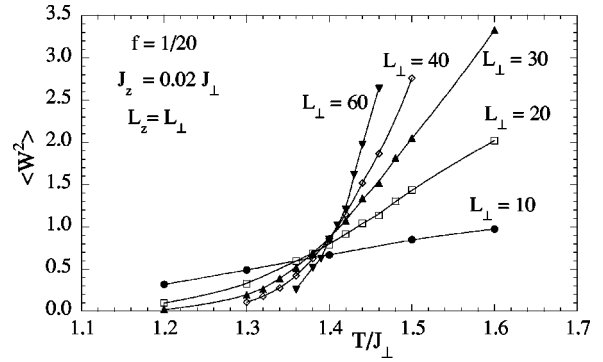


FIG. 2. Winding $\langle W^2 \rangle$ vs T/J_{\perp} for $L_{\perp} = 10, 20, 30, 40,$ and 60 , with vortex density $f = 1/20$, anisotropy $J_z = 0.02J_{\perp}$, and aspect ratio $L_z = L_{\perp}$. $\langle W^2 \rangle$ is computed using method (ii), i.e., we first find all percolating transverse loops. Curves of $\langle W^2 \rangle$ intersect at a common point, locating $T_{\Phi} \approx 1.4J_{\perp}$. Solid lines are guides to the eye only.

Fitting each of the curves of $\langle W^2 \rangle$ to a cubic polynomial in T , we compute their derivatives at the intersection point $T = 1.4J_{\perp}$, and plot the results vs L_{\perp} in Fig. 3. We see that the slopes, to an excellent approximation, scale linearly with L_{\perp} , thus suggesting a critical exponent $\nu \approx 1$. On closer inspection, the data in Fig. 3 show a small systematic downwards curvature about the linear fit; however, this curvature can be removed by assuming a slightly higher critical temperature of $T = 1.403J_{\perp}$. Note that this value of $\nu \approx 1$ is larger than the predicted value of $2/3$.

As an alternative method to compute the critical behavior, we can take the scaling Eq. (12), expand the scaling function $f(x)$ as a polynomial for small x , and do a nonlinear fitting to the data to determine the unknown polynomial coefficients, T_{Φ} and ν . To obtain the best fit we use a fourth-order polynomial and fit only the data from the two largest sizes, $L_{\perp} = 40$ and 60 . The results give $T_{\Phi} \approx 1.403J_{\perp}$ and $\nu \approx 0.96$, in agreement with the earlier estimates. In Fig. 4 we show the scaling collapse that results from this polynomial fit. There are systematic deviations from the fitted curve on the $T > T_{\Phi}$ side, though these appear to decrease as L_{\perp} increases.

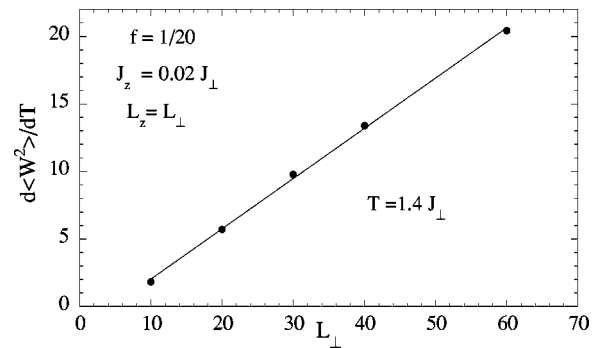


FIG. 3. Winding slopes $d\langle W^2 \rangle/dT$ vs L_{\perp} at the estimated crossing temperature of Fig. 2, $T = 1.4J_{\perp}$, for $L_{\perp} = 10, 20, 30, 40,$ and 60 , with vortex density $f = 1/20$, anisotropy $J_z = 0.02J_{\perp}$, and aspect ratio $L_z = L_{\perp}$. The solid line is the best linear fit to the data. The good fit suggests the critical exponent $\nu \approx 1$.

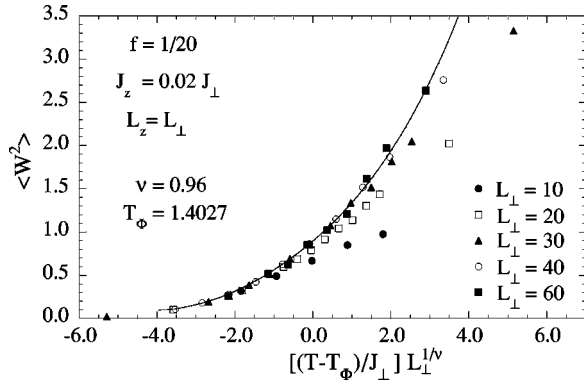


FIG. 4. Scaling collapse of data of Fig. 2. $\langle W_z^2 \rangle$ plotted vs $[(T - T_\Phi)/J_\perp] L_\perp^{1/\nu}$, for $L_\perp = 10, 20, 30, 40$, and 60 , with vortex density $f = 1/20$, anisotropy $J_z = 0.02 J_\perp$, and aspect ratio $L_z = L_\perp$. Data is fit to a polynomial expansion of Eq. (12), and $T_\Phi \approx 1.4027 J_\perp$ and $\nu \approx 0.96$ determined from the fit. Only data from $L_\perp = 40$ and 60 are used in the fit, although data from all sizes are shown in the plot. The solid line is the fitted polynomial curve.

Next we consider the excess parallel winding of the field-induced lines W_z . As discussed earlier, Tešanović's theory predicts a scaling of $\langle W_z^2 \rangle$ such as that in Eq. (14). To determine W_z we count the winding of vortex line paths $\{\alpha\}$ that wind negatively in the z direction, i.e., they have a net displacement of $R_{\alpha z} = -m_\alpha L_z$, with m_α a positive integer (\mathbf{R}_\perp may have any value for such paths). Since such negative parallel windings must be compensated for by excess field "lines," we have $W_z = \sum_\alpha m_\alpha$.

However, when we have used either of our tracing methods (i) or (ii), we have never found any such negative parallel windings up to the highest temperature we have simulated, $T = 1.6 J_\perp$. This has motivated us to define a third tracing scheme: (iii) we first search through all possible connections to find any paths with $R_{\alpha z} < 0$.

In Fig. 5 we show results, using tracing scheme (iii), for $\langle W_z^2 \rangle$ vs T/J_\perp for the same system parameters and sizes as used in Fig. 2 for $\langle W^2 \rangle$. Note that the values of $\langle W_z^2 \rangle$ at which the curves for different L_\perp intersect are exceedingly small. The intersection points appear to decrease in T as L_\perp increases, however, we are not able to make any firm conclusions.

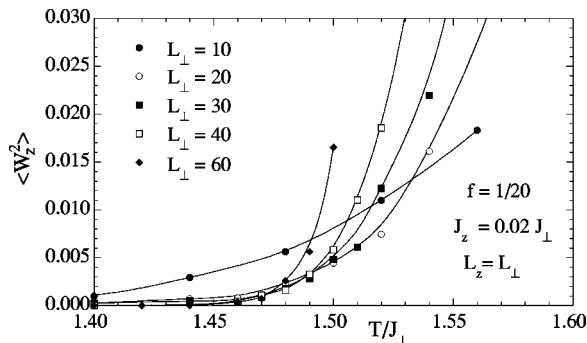


FIG. 5. z axis winding $\langle W_z^2 \rangle$ vs T/J_\perp for $L_\perp = 10, 20, 30, 40$, and 60 , with vortex density $f = 1/20$, anisotropy $J_z = 0.02 J_\perp$, and aspect ratio $L_z = L_\perp$. $\langle W_z^2 \rangle$ is computed using method (iii), i.e., we first find all loops that percolate in the negative \hat{z} direction. Solid lines are guides to the eye only.

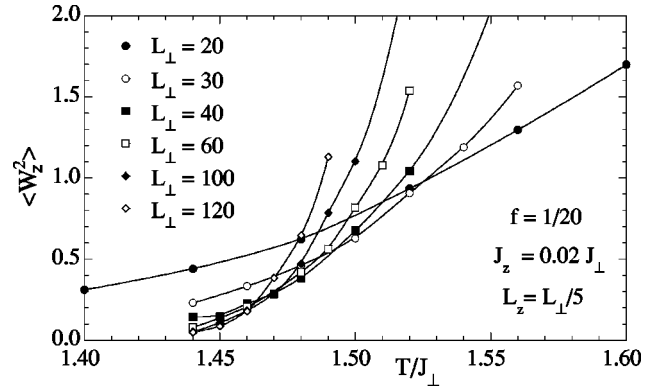


FIG. 6. z axis winding $\langle W_z^2 \rangle$ vs T/J_\perp for $L_\perp = 20, 30, 40, 60, 100$, and 120 , with vortex density $f = 1/20$, anisotropy $J_z = 0.02 J_\perp$, and aspect ratio $L_z = L_\perp/5$. $\langle W_z^2 \rangle$ is computed using method (iii), i.e., we first find all loops that percolate in the negative \hat{z} direction. Solid lines are guides to the eye only.

In an attempt to improve the analysis of $\langle W_z^2 \rangle$ we have repeated the calculation, using a new system aspect ratio of $L_z = L_\perp/5$. This has the effect of increasing the value at which the curves of $\langle W_z^2 \rangle$ intersect, hopefully improving our accuracy. We have explicitly checked that changing the aspect ratio does not shift the transition temperature T_Φ observed in $\langle W^2 \rangle$ (see also Sec. IV B). In Fig. 6 we show results for $\langle W_z^2 \rangle$ vs T/J_\perp for this new aspect ratio. Again we find no common intersection point for the sizes considered. As L_\perp increases, the intersection point continues to decrease. Whether this is a result of a failure of the scaling hypothesis of Eq. (14), or whether we have simply failed to reach the scaling limit of sufficiently large L_z ($L_z = 24$ is the largest value in Fig. 6), we cannot be certain. Note that in both Figs. 5 and 6, $\langle W_z^2 \rangle$ appears to be vanishing at a temperature noticeably above $T_\Phi \approx 1.4 J_\perp$, where the curves of the transverse winding, $\langle W^2 \rangle$, intersect.

We have also tried to fit the data of Fig. 6 to the scaling form $\langle W_z^2 \rangle \sim L^{-x} f_z(t L_\perp^{1/\nu})$, assuming a nontrivial anomalous scaling dimension x (although we have no specific theoretical reason to propose this form). When we do so, we obtain $T_c = 1.44$, $\nu = 0.76$, and $x = 1.185$, however, our data in the vicinity of this T_c is too scattered for us to place much significance on this fit.

Having used tracing method (iii) to first eliminate all possible lines percolating in the negative \hat{z} direction, we can then search for all possible transversely percolating lines and compute the resulting transverse winding $\langle W^2 \rangle$. When we do this, we find our results for $\langle W^2 \rangle$ virtually unchanged from tracing method (ii) in the vicinity of $T_\Phi \approx 1.4 J_\perp$. The extremely low number of negative \hat{z} percolating lines at this temperature produces no noticeable effect on the transverse tracing.

IV. PERCOLATING LOOPS

A. Summary of Nguyen and co-workers' method

As discussed in the preceding Section III.A, a transition at T_Φ would mark the appearance of infinite transverse loops,

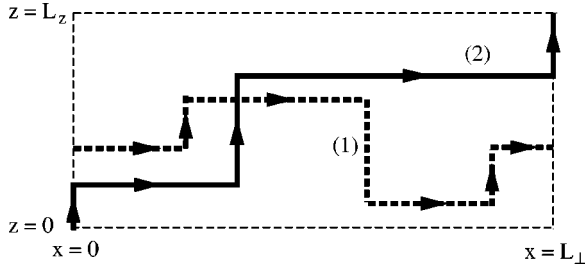


FIG. 7. Percolating transverse vortex paths. Path (1) closes upon itself without ever winding about the system in the \hat{z} direction. Path (2) only closes upon itself after winding once in the \hat{z} direction. Both paths contribute to the calculation of O'_L by method (ii'). Only path (1) contributes to the calculation of O_L by method (ii). The thin dashed lines represent the periodic boundaries of the system.

as T is increased. The idea to explicitly look for transverse paths that percolate across the system was first put forth by Jagla and Balseiro.²¹ Later, Nguyen and co-workers^{8–10} refined this idea. They defined a quantity which they denoted O_L , that is the probability that a vortex path exists which travels completely across the system in a direction transverse to the applied magnetic field, without ever traveling completely across the system in the direction parallel to the field. If such a path exists in a given configuration, that configuration counts as unity in the average for O_L ; if not, that configuration counts as zero.

Since having $W^2 > 0$ in a given configuration necessarily implies that there is a percolating transverse loop in that configuration, there is a close connection between the quantities $\langle W^2 \rangle$ and O_L . They differ in that (i) for a configuration with $W^2 > 1$, and hence with more than one percolating transverse loop, the contribution to O_L remains unity, rather than increasing with the number of percolating transverse loops; and (ii) in a configuration with two percolating but oppositely oriented transverse loops, the contribution to O_L will be unity, but these loops cancel each other in their contribution to W^2 , which might therefore be zero.

Since O_L is a pure number one might expect it to be a scale-invariant quantity, and hence, similarly to $\langle W^2 \rangle$, plots of O_L vs T for different system sizes L_\perp should have a common intersection point at T_ϕ . Nguyen and co-workers' method of searching for such percolating transverse paths is similar to our method (ii) except for one crucial difference.²² They do not require that the transverse path close upon itself; they only require that the path start at one end of the system, say, at $x=0$, and continue until reaching the opposite end, $x=L_\perp$, while keeping the distance traveled along \hat{z} less than L_z , that is, the displacement traveled along the path α satisfies $R_{x\alpha} = L_\perp$ and $R_{z\alpha} < L_z$. Since, by the periodic boundary conditions, all paths *must* eventually close upon themselves, there are two possibilities for the transverse percolating paths that Nguyen and co-workers find. We illustrate these in Fig. 7: (1) the path α eventually closes upon itself without ever traveling the length L_z , in which case $R_{z\alpha} = 0$; or (2) the path α , when followed until it closes upon itself, winds up traveling the length L_z , with a displacement $R_{z\alpha} = L_z$; in this

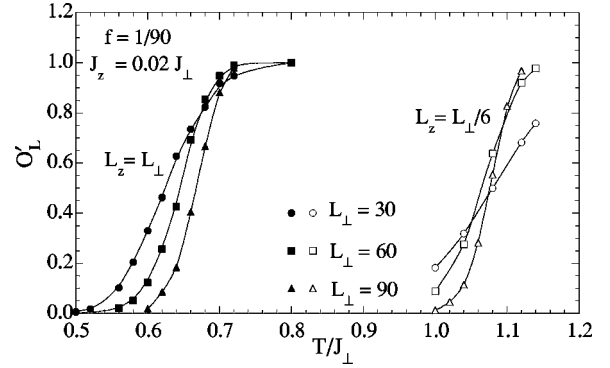


FIG. 8. Percolation probability O'_L vs T/J_\perp for $L_\perp = 30, 60,$ and 90 , with vortex density $f = 1/90$ and anisotropy $J_z = 0.02J_\perp$. Solid symbols on the left are for aspect ratio $L_z = L_\perp$; open symbols on the right are for aspect ratio $L_z = L_\perp/6$. O'_L is computed using method (ii'), following Nguyen and co-workers. Solid lines are guides to the eye only.

case, our method (ii) would consider this path as part of the field-induced vortex lines $n_{s\mu}^{\text{lines}}$, contributing to the winding \mathbf{W} , rather than as a transverse loop that contributes to $n_{s\mu}^{\text{loops}}$. We call Nguyen and co-workers' path tracing method (ii') to distinguish it from our method (ii). We denote by O'_L the probability for a percolating path using method (ii'); using method (ii) we denote it by O_L . Paths of type (2) will contribute to O'_L , but not to O_L . We will see that there are very dramatic differences between these two methods, and that only O_L gives self-consistent results.

B. Numerical results

First, we note that if we use method (i) (random connections) to search for percolating transverse paths, the result will essentially be the same as found for $\langle W^2 \rangle$ in Sec. III B. As L_\perp increases, the probability of finding a percolating transverse loop steadily decreases for the entire temperature range, becoming immeasurably small for our biggest system size. Hence we will focus here on methods (ii) and (ii').

We now consider the computation of O'_L using method (ii'), the one used by Nguyen and co-workers, which never checks the way in which the percolating transverse path closes upon itself. We first use parameters $J_z = 0.02J_\perp$ and $L_z = L_\perp$, the same as those in Sec. III B, but a more dilute density of vortex lines $f = 1/90$. For these parameters, the vortex lattice melting temperature is $T_m \approx 0.49J_\perp$, and the zero-field critical temperature, as before, is $T_{c0} \approx 1.14J_\perp$. These parameters are very close to the parameters of one of the cases studied by Nguyen and co-workers in Refs. 9 and 10 [they used $f = 1/90$, $J_z = (1/49)J_\perp$, and $L_z \sim L_\perp$]. Our results for O'_L vs T/J_\perp , for three system sizes, $L_\perp = 30, 60,$ and 90 , are shown as the solid symbols on the left-hand side of Fig. 8. These results agree quite closely with those of Nguyen and co-workers (see Fig. 8 of Ref. 9), and seem to show what might be a common intersection of the three curves near $T \approx 0.7J_\perp$. However, we now consider the same parameters and sizes L_\perp , only using a different system aspect ratio, $L_z = L_\perp/6$. The results are shown as the open sym-

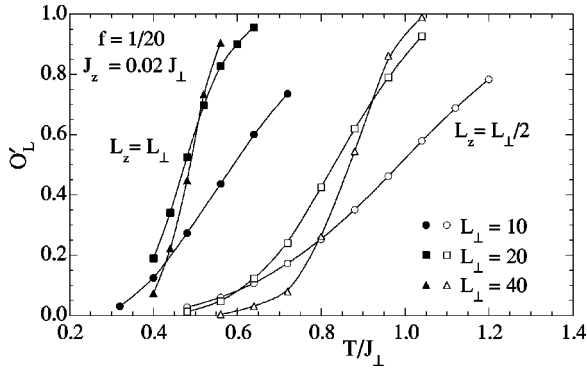


FIG. 9. Percolation probability O'_L vs T/J_\perp for $L_\perp = 10, 20,$ and 40 , with vortex density $f = 1/20$ and anisotropy $J_z = 0.02J_\perp$. Solid symbols on the left are for aspect ratio $L_z = L_\perp$; open symbols on the right are for aspect ratio $L_z = L_\perp/2$. O'_L is computed using method (ii'), following Nguyen and co-workers. Solid lines are guides to the eye only.

bols on the right-hand side of Fig. 8. We see that there no longer appears to be a common intersection point, but more importantly, the curves have all shifted dramatically to higher temperatures. Thus, any value of T_Φ that one might try to extract from O'_L depends sensitively on the system aspect ratio. We have also considered other values of the aspect ratio L_z/L_\perp , not shown here. The clear trend is that the sharp rise in O'_L shifts to increasing temperatures as L_z/L_\perp decreases. But if T_Φ represents a true phase transition, it must be *independent* of aspect ratio. We therefore conclude that O'_L and method (ii') do not give any self-consistent evidence of the proposed vortex loop blowout transition.

The problems with O'_L are even clearer if we consider the parameters $f = 1/20$ and $J_z = 0.02J_\perp$, the same ones used for our computation of $\langle W^2 \rangle$ in Sec. III B. In Fig. 9 we show our results for $L_\perp = 10, 20,$ and 40 , for the two aspect ratios $L_z = L_\perp$ and $L_z = L_\perp/2$. In both cases, there is no common intersection point of the three curves for the three sizes, and the curves for the smaller aspect ratio are shifted to higher temperatures. Note also that, for both aspect ratios, the temperatures at which O'_L rises to unity lie quite significantly below the value of $T_\Phi \approx 1.4J_\perp$ found from our analysis of $\langle W^2 \rangle$.

We next consider the computation of O_L using method (ii) (the percolating transverse path must close upon itself keeping $R_{z\alpha} = 0$). In Fig. 10 we show results using the same parameters as were used to compute O'_L in Fig. 8, i.e., $f = 1/90$, $J_z = 0.02J_\perp$, and $L_\perp = 30, 60$ and 90 , for the same two aspect ratios $L_z = L_\perp$ and $L_z = L_\perp/6$. We see now that for both aspect ratios, curves for the three different sizes appear to approach a common intersection point, $T_\Phi \approx 1.17J_\perp > T_{c0} \approx 1.14J_\perp$, and that this intersection point is independent of aspect ratio (note that for $L_z = L_\perp/6$, the thinness of the system $L_z = 5$, for $L_\perp = 30$, presumably makes it too small to be in the scaling region, hence it intersects the other two curves at somewhat lower temperatures).

In Fig. 11 we show similar results using the same parameters as were used in our computation of $\langle W^2 \rangle$ in Sec. III B, i.e., $f = 1/20$, $J_z = 0.02J_\perp$, and $L_z = L_\perp$. We see that the

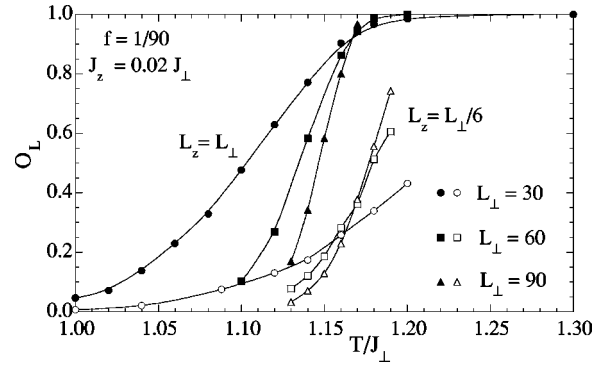


FIG. 10. Percolation probability O_L vs T/J_\perp for $L_\perp = 30, 60,$ and 90 with vortex density $f = 1/90$, and anisotropy $J_z = 0.02J_\perp$. Solid symbols are for aspect ratio $L_z = L_\perp$; open symbols are for aspect ratio $L_z = L_\perp/6$. O_L is computed using method (ii), where all loops close upon themselves. All curves approach a common intersection point, $T_\Phi \approx 1.17J_\perp$, independent of the aspect ratio. Solid lines are guides to the eye only.

curves of O_L vs T/J_\perp for the different system sizes $L_\perp = 10, 20, 30,$ and 40 all intersect at a common point, $T_\Phi \approx 1.4J_\perp$. This is exactly the same value as found in our analysis of $\langle W^2 \rangle$ (see Fig. 2).

We therefore conclude that O_L gives a self-consistent determination of T_Φ , and that this value is considerably larger than estimates considering O'_L . In fact, estimates of T_Φ from O'_L all lie *below* the zero-field critical temperature T_{c0} and *decrease* as f increases, while the values determined from O_L all lie *above* T_{c0} , and *increase* as f increases.

If O_L is indeed a scale-invariant quantity, we can postulate that it should obey a scaling relation similar to $\langle W^2 \rangle$, i.e.,

$$O_L(T, L_\perp) = \tilde{f}(tL^{1/\nu}). \quad (15)$$

Based on our analysis of $\langle W^2 \rangle$ in Sec. III B, we may expect $\nu \approx 1$. In Fig. 12 we therefore show a scaling collapse of the data for $f = 1/90$ from Fig. 10, plotting O_L vs $[(T$

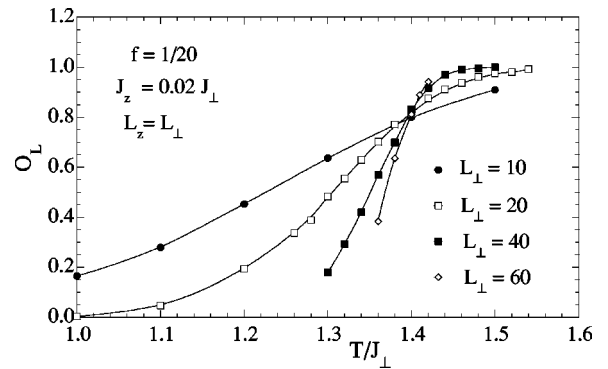


FIG. 11. Percolation probability O_L vs T/J_\perp for $L_\perp = 10, 20, 40,$ and 60 , with vortex density $f = 1/20$, anisotropy $J_z = 0.02J_\perp$, and aspect ratio $L_z = L_\perp$. O_L is computed using method (ii), where all loops close upon themselves. All curves approach a common intersection point, $T_\Phi \approx 1.4J_\perp$, in agreement with the analysis of $\langle W^2 \rangle$ in Fig. 2. Solid lines are guides to the eye only.

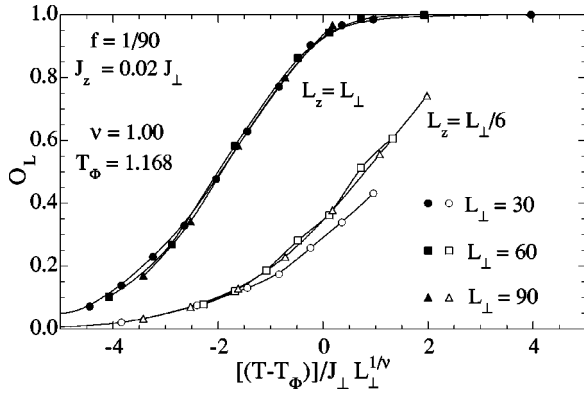


FIG. 12. Scaling collapse O_L vs $[(T-T_\Phi)/J_\perp]L_\perp^{1/\nu}$ of data from Fig. 10, for $f=1/90$. A reasonably good collapse is found for all sizes L_\perp , for both aspect ratios L_z/L_\perp , using a single value of $T_\Phi \approx 1.168J_\perp$ and $\nu=1$. Solid lines are guides to the eye only.

$-T_\Phi)/J_\perp]L_\perp$, where T_Φ is determined by a best fit of the data to the scaling form. We find a reasonably good collapse for all sizes, for both aspect ratios, using a single value of $T_\Phi \approx 1.168J_\perp$.

In Fig. 13 we show a similar scaling collapse of the data for $f=1/20$ from Fig. 11. Fitting the data for O_L to a fourth-order polynomial expansion of the scaling function, we find an excellent collapse, for all system sizes, using the parameters $T_\Phi \approx 1.399J_\perp$ and $\nu=1.006$. These results agree very well with the values obtained from the scaling analysis of $\langle W^2 \rangle$, given in Sec. III B. The quality of the collapse is much better here than it was for $\langle W^2 \rangle$ in Fig. 4.

Finally, in analogy with the winding $\langle W_z^2 \rangle$, we have also considered the probability O_{L_z} to find a vortex path percolating through the system in the negative \hat{z} direction, opposite to the applied magnetic field. We expect O_{L_z} to obey a scaling relation similar to that of Eq. (15). To compute O_{L_z} we have used tracing method (iii) in which we explicitly search through all possible connections to find any such paths. We show our results for O_{L_z} vs T/J_\perp for vortex density $f=1/20$ and anisotropy $J_z=0.02J_\perp$ in Figs. 14 and 15,

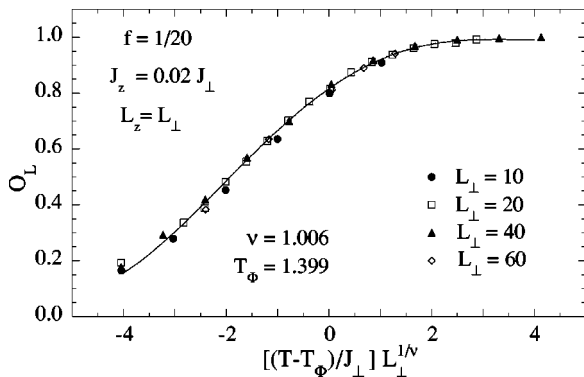


FIG. 13. Scaling collapse O_L vs $[(T-T_\Phi)/J_\perp]L_\perp^{1/\nu}$ of data from Fig. 11, for $f=1/20$. An excellent collapse is found for all sizes L_\perp , using values of $T_\Phi \approx 1.399J_\perp$ and $\nu=1.006$. These values agree well with those obtained from the scaling collapse of $\langle W^2 \rangle$. The solid line is the fitted polynomial curve.

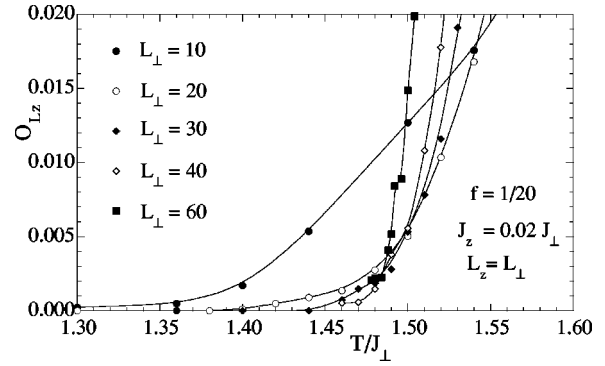


FIG. 14. Percolation probability O_{L_z} vs T/J_\perp for $L_\perp=10, 20, 30, 40,$ and 60 , with vortex density $f=1/20$, anisotropy $J_z=0.02J_\perp$, and aspect ratio $L_z=L_\perp$. O_{L_z} is computed using tracing method (iii). Solid lines are guides to the eye only.

for system aspect ratios $L_z=L_\perp$ and $L_z=L_\perp/5$, respectively. As with $\langle W_z^2 \rangle$ shown in Figs. 5 and 6, the intersection points of the curves for different sizes appear to decrease in temperature as L_\perp increases. Again, we cannot say whether this is a failure of our scaling hypothesis or a failure to reach sufficiently large L_z . Also, analogous to our findings for the windings $\langle W^2 \rangle$ and $\langle W_z^2 \rangle$, O_{L_z} appears to be vanishing at a temperature above $T_\Phi=1.4J_\perp$ where the curves of O_L intersect.

V. SPECIFIC HEAT

If T_Φ , as determined by $\langle W^2 \rangle$ or O_L , does indeed represents a true thermodynamic transition, we would expect to see some signature of this transition in more conventional thermodynamic quantities. In the recent experiments of Ref. 11, a steplike anomaly in the specific heat C was observed in the vortex line liquid region, reminiscent of an inverted mean-field transition. In their numerical simulations,^{9,10} Nguyen and Sudbø claimed to see an anomalous glitch in the specific heat at the temperature they identified as T_Φ from their calculation of O'_L . However, this glitch corresponded to only a single data point very slightly displaced above an otherwise smooth background, and in the previous section

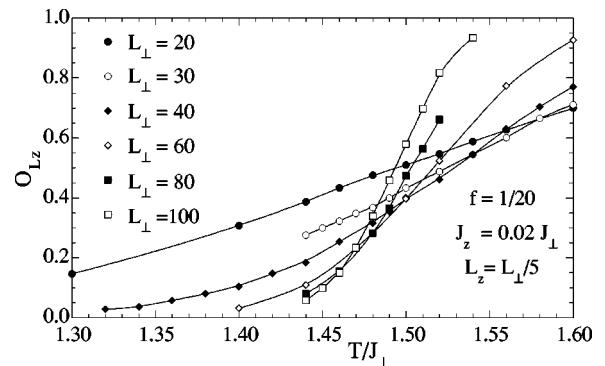


FIG. 15. Percolation probability O_{L_z} vs T/J_\perp for $L_\perp=20, 30, 40, 60, 80,$ and 100 , with vortex density $f=1/20$, anisotropy $J_z=0.02J_\perp$, and aspect ratio $L_z=L_\perp/5$. O_{L_z} is computed using tracing method (iii). Solid lines are guides to the eye only.

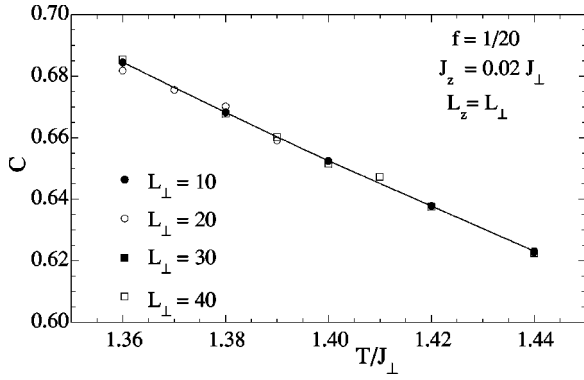


FIG. 16. Specific heat C vs T/J_{\perp} for vortex density $f=1/20$, anisotropy $J_z=0.02J_{\perp}$, and aspect ratio $L_z=L_{\perp}$, for system sizes $L_{\perp}=10, 20, 30$, and 40 . No hint of any anomaly is found near the previously determined $T_{\Phi}\approx 1.4J_{\perp}$. The solid line is a guide to the eye only.

we have demonstrated that O'_L significantly underestimates T_{Φ} , hence there is no reason to expect any anomaly in C at that temperature.

In this section we report on high-precision measurements of the specific heat C , for the same parameters we have studied in the earlier sections. If T_{Φ} , as found using the vortex path tracing method (ii), is indeed a true thermodynamic phase transition with critical exponent $\nu\approx 1$ (as our scaling analyses found), then hyperscaling would suggest a specific-heat exponent of $\alpha=2-d\nu\approx -1$. We thus do not expect to see a diverging C , however, some feature should be present.

In Fig. 16 we plot C vs T/J_{\perp} , in the vicinity near $T_{\Phi}\approx 1.4J_{\perp}$, for the same parameters $f=1/20$, $J_z=0.02J_{\perp}$, and $L_z=L_{\perp}$ as used in Figs. 2, 11, and 13. We show results for $L_{\perp}=10, 20, 30$, and 40 , using $3-10\times 10^7$ Monte Carlo passes through the lattice, depending on the system size. We find no noticeable finite-size dependence, and no hint of any feature at all, near the previously determined $T_{\Phi}\approx 1.4J_{\perp}$.

In Fig. 17 we plot C vs T/J_{\perp} , over a broad temperature range, for the same parameters $f=1/90$ and $J_z=0.02J_{\perp}$ as used in Figs. 10 and 12, but for a single large system size $L_{\perp}=30$ and $L_z=90$. Again we see no hint of any anomaly near the previously determined $T_{\Phi}\approx 1.168J_{\perp}$.

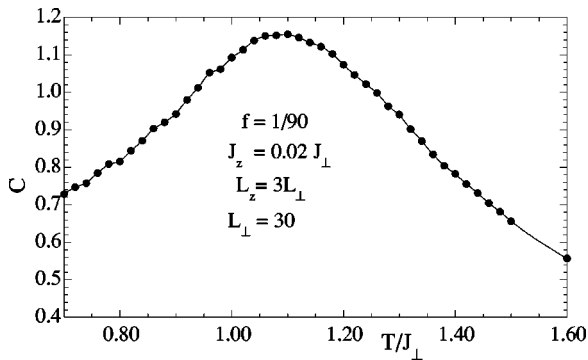


FIG. 17. Specific heat C vs T/J_{\perp} for vortex density $f=1/90$, anisotropy $J_z=0.02J_{\perp}$, and aspect ratio $L_z=3L_{\perp}$, for system size $L_{\perp}=30$. No hint of any anomaly is found near the previously determined $T_{\Phi}\approx 1.168J_{\perp}$. The solid line is a guide to the eye only.

VI. CONCLUSIONS

We have carried out detailed Monte Carlo investigations of the 3D uniformly frustrated XY model in order to search for a proposed “vortex loop blowout” transition within the vortex line liquid phase of a pure extreme type-II superconductor. Such a transition had been predicted as a result of general theoretical arguments by Tešanović.⁷ Evidence for such a transition was claimed in numerical simulations by Nguyen and co-workers,⁸⁻¹⁰ and in specific-heat measurements on high purity YBCO single crystals.¹¹ We have made explicit measurements of the vortex line windings $\langle W^2 \rangle$ and $\langle W_z^2 \rangle$, which are the key quantities in Tešanović’s theory. We have reexamined Nguyen and co-workers’ calculation of the percolation probability O_L .

Our results raise several questions concerning Tešanović’s theory. We have found that the values of $\langle W^2 \rangle$ and $\langle W_z^2 \rangle$ depend sensitively on the precise scheme one uses to trace vortex line paths. For the natural choice of random connectivity at vortex line intersections, both $\langle W^2 \rangle$ and $\langle W_z^2 \rangle$ appear to vanish at all temperatures as $L\rightarrow\infty$. Only when we specifically search first for percolating paths, when computing the windings, do we find that the windings converge to nonzero values above a certain temperature. In this case, we find that the transverse winding $\langle W^2 \rangle$ obeys the finite-size scaling form expected from Tešanović’s theory, however, the critical exponent we find is $\nu\approx 1$, rather than the predicted $\nu_{XY}\sim 2/3$ of the inverted 3D XY transition. For the longitudinal winding $\langle W_z^2 \rangle$ we have been unable to find the expected scaling form. Whether this is because $\langle W_z^2 \rangle$ does not scale, or because our systems are all too small to be in the scaling limit, we cannot be certain. It does appear that, upon cooling, $\langle W_z^2 \rangle$ vanishes at a temperature above that at which $\langle W^2 \rangle$ vanishes. This would be contrary to Tešanović’s theory. However, since we have not succeeded in finding scaling for $\langle W_z^2 \rangle$, we cannot be certain of knowing exactly where it vanishes as $L\rightarrow\infty$.

Independent of Tešanović’s theory, it is natural to think that, as temperature and hence vorticity increase, the vortex lines may form percolating paths (note, however, that the directedness of the vortex line segments and the condition of divergenceless paths means that this is no ordinary percolation problem). We have therefore, following Nguyen and co-workers, searched explicitly for such percolating paths in the direction transverse to the applied magnetic field, as well as in the direction parallel but opposite to the applied magnetic field. Defining transverse percolation as the existence of a vortex line path that extends entirely across the system in the direction transverse to the applied magnetic field *without* simultaneously extending entirely across the system in the parallel direction, we have shown that Nguyen and co-workers’ procedure, which ignores the transverse periodic boundary conditions and does not require the percolating path to close upon itself, leads to inconsistent predictions for the transition temperature as one varies the system aspect ratio. Only by requiring that the transverse percolating path close upon itself, *without* ever winding in the parallel direction, do we find a consistent transition temperature independent of aspect ratio. The percolation transition found this way agrees both

in critical temperature T_Φ and exponent ν with the results from our analysis of the transverse winding $\langle W^2 \rangle$. We have also computed the probability of finding a percolating path in the direction parallel but opposite to the applied magnetic field. Here, analogous to our results for $\langle W_z^2 \rangle$, this negative \hat{z} percolation appears to occur at a temperature higher than that of the transverse percolation, however, we have not succeeded in finding a clear scaling of this parallel percolation probability.

Note that the transverse percolation transition temperature $T_\Phi(f)$ that we find *increases* above the zero-field transition temperature T_{c0} as the magnetic-flux density f *increases*. This is in striking contrast to the conclusion of Nguyen and co-workers who proposed $T_\Phi(f)$ to *decrease* below T_{c0} as f *increases*.

While our results do seem consistent with a well-defined transverse percolation transition, one can ask if this is a purely geometrical feature of the vortex line paths, or whether it also corresponds to a true thermodynamic phase transition, i.e., something one could detect in a suitable thermodynamic derivative of the free energy. To investigate this question we have carried out high-precision Monte Carlo measurements of the specific heat C . Our results for C show

no feature whatsoever near the percolation transition T_Φ , nor do we find any finite-size effect. In particular we see no evidence for a steplike feature as was observed experimentally in YBCO.

To conclude, we have found evidence for a well-defined transverse percolation temperature within the vortex line liquid phase of a model type-II superconductor. The connection between this transition and Tešanović's theory of a vortex loop "blowout" transition remains unclear. It also remains unclear whether or not this percolation transition has any observable thermodynamic manifestation.

ACKNOWLEDGMENTS

We would like to thank Professor Z. Tešanović and Professor A. Sudbó for many helpful conversations. This work was supported by the Engineering Research Program of the Office of Basic Energy Sciences at the Department of Energy, Grant No. DE-FG02-89ER14017, the Swedish Natural Science Research Council Contract No. E 5106-1643/1999, and by the resources of the Swedish High Performance Computing Center North (HPC2N). Travel between Rochester and Umeå was supported by Grant Nos. NSF INT-9901379 and STINT 99/976(00).

¹E. Zeldov, D. Majer, M. Konczykowski, V. B. Geshkenbein, V. M. Vinokur, and H. Strikman, *Nature (London)* **375**, 373 (1995); A. Schilling, R. A. Fisher, N. E. Phillips, U. Welp, D. Dasgupta, W. K. Kwok, and G. W. Crabtree, *ibid.* **382**, 791 (1996).

²M. V. Feigel'man, V. B. Geshkenbein, L. B. Ioffe, and A. I. Larkin, *Phys. Rev. B* **48**, 16 641 (1993).

³Y.-H. Li and S. Teitel, *Phys. Rev. B* **47**, 359 (1993).

⁴Y.-H. Li and S. Teitel, *Phys. Rev. B* **49**, 4136 (1994).

⁵T. Chen and S. Teitel, *Phys. Rev. B* **55**, 11 766 (1997); S. Ryu and D. Stroud, *Phys. Rev. B* **57**, 14 476 (1998).

⁶X. Hu, S. Miyashita, and M. Tachiki, *Phys. Rev. Lett.* **79**, 3498 (1997); *Phys. Rev. B* **58**, 3438 (1998); A. K. Nguyen and A. Sudbó, *ibid.* **58**, 2802 (1998); P. Olsson and S. Teitel, *Phys. Rev. Lett.* **82**, 2183 (1999).

⁷Z. Tešanović, *Phys. Rev. B* **59**, 6449 (1999); **51**, 16 204 (1995).

⁸S. K. Chin, A. K. Nguyen, and A. Sudbó, *Phys. Rev. B* **59**, 14 017 (1999).

⁹A. K. Nguyen and A. Sudbó, *Europhys. Lett.* **46**, 780 (1999).

¹⁰A. K. Nguyen and A. Sudbó, *Phys. Rev. B* **60**, 15 307 (1999).

¹¹F. Bouquet, C. Marcenat, E. Steep, R. Calemczuk, W. K. Kwok, U. Welp, G. W. Crabtree, R. A. Fisher, N. E. Phillips, and A. Schilling, *Nature (London)* **411**, 448 (2001).

¹²Y.-H. Li and S. Teitel, *Phys. Rev. Lett.* **66**, 3301 (1991).

¹³P. Olsson, *Europhys. Lett.* **58**, 705 (2002).

¹⁴For large systems, it is crucial to have an efficient algorithm to search for such paths. We use the following. First, all intersection points are located. Picking one such point at random, we trace a path starting from this intersection point until it arrives at another intersection point. If the height traveled from the starting

to the new intersection point is $\Delta z > 0$, we stop this search and start again at a different intersection point; if not, we continue tracing the path until then next intersection point is encountered and then repeat the height test. Since most paths connect to field lines which travel in the $+z$ direction, most such tracings are quickly aborted. However, since each possible transverse loop with $R_{z\alpha} = 0$ contains an intersection point that is at the largest height of all intersection points on that loop, we are guaranteed to ultimately find this path with this search algorithm.

¹⁵C. Dasgupta and B. I. Halperin, *Phys. Rev. Lett.* **47**, 1556 (1981).

¹⁶E. Fradkin, B. Huberman, and S. Shenker, *Phys. Rev. B* **18**, 4789 (1978); G. Carneiro, *ibid.* **45**, 2391 (1992).

¹⁷T. Chen and S. Teitel, *Phys. Rev. B* **55**, 15 197 (1997).

¹⁸M. Kiometzis, H. Kleinert, and A. M. J. Schakel, *Fortschr. Phys.* **43**, 697 (1995).

¹⁹P. Olsson and S. Teitel, *Phys. Rev. Lett.* **80**, 1964 (1998).

²⁰D. R. Nelson, *Phys. Rev. Lett.* **60**, 1973 (1988); *J. Stat. Phys.* **57**, 511 (1989); D. R. Nelson and S. Seung, *Phys. Rev. B* **39**, 9153 (1989).

²¹E. A. Jagla and C. A. Balseiro, *Phys. Rev. B* **53**, R538 (1996); *ibid.* **53**, 15 305 (1996). In these works, the authors considered *all* transverse percolating loops, including those with net winding in the parallel direction, $R_{\alpha z} > 0$. One can show (see Ryu and Stroud in Ref. 5) that the onset of such loops, which in general involve the participation of the field-induced lines and so have $R_{\alpha z} > 0$, coincides with the vanishing of the longitudinal helicity modulus and occurs at the melting T_m , rather than the proposed T_Φ . Only by restricting to loops with $R_{\alpha z} = 0$ does one probe T_Φ .

²²A. Sudbó (private communication).